Positron production in a laser plasma for measuring superhigh laser intensities

I. A. Aleksandrov and A. A. Andreev
Department of Physics, St. Petersburg State University, Universitetskaya Naberezhnaya 7/9, Saint Petersburg 199034, Russia and Ioffe Institute, Politekhnicheskaya Street 26, Saint Petersburg 194021, Russia

(Received 16 March 2024; accepted 25 June 2024; published 11 July 2024)

Quantum electrodynamics (QED) predicts the phenomenon of electron-positron pair production via the decay of a high-energy photon in the presence of strong external fields. Such photons can be generated due to nonlinear Compton scattering involving electrons propagating in an intense external background. Here we investigate the possibility of extracting superhigh laser intensities by measuring the positron yield. Our numerical simulations based on the QED rates of the two aforementioned processes provide the total number of positrons as a function of the laser intensity for two different setups: a single focused laser pulse and a combination of two counterpropagating pulses. As seed particles, we consider a free-electron gas and a gas of neutral Xe atoms. In this study, special focus is placed on taking into account the cascade process of pair production, which can occur in the case of superhigh laser intensities. It is demonstrated that the contribution of the QED cascade is not important in the vicinity of the positron generation threshold; i.e., an extended intensity domain where the laser field produces a substantial number of positrons but does not yet launch the cascade exists. Within this range, the intensity diagnostics is particularly accurate. By adjusting the geometry of the experimental setup, one can change the corresponding threshold value of the laser intensity in order to maximize the accuracy of the diagnostic scheme.

DOI: 10.1103/PhysRevA.110.013111

I. INTRODUCTION

Rapid developments in laser technologies have excited great interest in both theoretical and experimental studies of various QED phenomena in strong fields. An intensity of $10^{23}\,\mathrm{W/cm^2}$ was already achieved [1], and one can expect that laser intensity in real experiments will soon exceed $10^{24}\,\mathrm{W/cm^2}$, opening up the possibility of probing QED in extremely intense backgrounds (see, e.g., recent reviews [2,3]). Nevertheless, an accurate determination of the laser intensity represents a challenging task. There are several proposals in the literature based on investigating the ionization process of highly charged ions [4–6], light scattering or additional radiation due to the interaction between electrons and the laser field [7–12], spin effects in electron beam scattering [13], photoionization, or direct acceleration of charged particles [14–23] (see also references therein).

In this paper, we examine the approach based on extracting the laser intensity by measuring the total number of positrons generated in the field of high-intensity lasers. Using these measurements, one can recover the laser intensity by means of one-to-one correspondences deduced in our recent study [24]. This kind of laser diagnostics can be quite accurate due to the threshold behavior of the pair-production process as a function of the field strength. In the present study, we report more accurate predictions taking into account the QED cascade process and explore the effects of the laser-field focusing in order to optimize the diagnostic technique.

Positron production occurs due to the decay of a high-energy photon in a strong external field. Such photons should be emitted via nonlinear Compton scattering by a high-energy electron or positron. This means that the particles produced can, in principle, be accelerated again in the external field and afterwards emit high-energy photons, so that the process of positron production represents a cascade (for a review, see, e.g., Ref. [25]). Unlike the so-called S-type ("shower") cascades in which the $e^+e^-\gamma$ production processes basically consume energy from the seed high-energy particles, the phenomenon under consideration may correspond to A-type ("avalanche") cascades (see, e.g., Refs. [26,27]). Here the external laser field not only serves as a background for the Compton and Breit-Wheeler mechanisms but also accelerates particles, so that they regain the energy lost. If the external field is sufficiently strong that the acceleration time t_{acc} and the electron and photon lifetimes $t_{e,\gamma}$ are much smaller than the interaction time t_{esc}, then a continuous avalanchelike reaction occurs, limited only by the laser pulse duration and ponderomotive expulsion of the particles.

Nevertheless, as we are mainly interested in pair production in external fields of intensity of 10^{22}–$10^{23}\,\mathrm{W/cm^2}$, the field is not strong enough to cause an A-type cascade, which can occur if $I \gtrsim 10^{24}\,\mathrm{W/cm^2}$ in the case of a standing electromagnetic wave [26–31]. More specifically, as demonstrated in Refs. [26,27], the hierarchy $t_{\mathrm{acc}} \ll t_{e,\gamma} \ll t_{\mathrm{esc}}$ takes place when at least $\mu \equiv E_0/(\alpha E_{\mathrm{c}}) \gtrsim 1$, where E_0 is the field amplitude, $E_{\mathrm{c}} = m^2c^3/|e\hbar| \approx 1.3 \times 10^{18}\,\mathrm{V/m}$ is the critical (Schwinger) field strength, and $\alpha \approx 1/137$ is the fine-structure constant. In our case, $\mu = 0.04$–0.28 for $I = 2 \times 10^{22}$–$10^{24}\,\mathrm{W/cm^2}$. Moreover, the second condition, $\mu^{1/4} \gg (1/\alpha)\sqrt{\hbar\omega/(mc^2)}$ (ω is the field frequency) from Refs. [26,27] is not satisfied either. This means that the exponential enhancement of the positron number due to the later stages of cascading is unlikely to take place in our case. However, to verify this quantitatively and explore different field

configurations, we will incorporate the QED cascade within our numerical simulations. In the present study, we examine a single focused laser pulse and a combination of two counterpropagating laser pulses. To describe the cascade process, instead of calculating the total number of pairs produced by a photon via the Breit-Wheeler mechanism, we will compute the probability of pair production at each time instant and then propagate the particles again while taking into account this probability as well as the weight of the photon itself. The corresponding recursive procedure developed in the present study allows us to take into account the necessary number of successive stages of the QED cascade.

This paper has the following structure. In Sec. II we describe the experimental setup specifying the parameters of the laser field and seed particles. In Sec. III we outline our numerical approach, placing emphasis on the recursive procedure allowing one to take into account QED cascades. Section IV contains the main results of our study. Finally, we conclude in Sec. V.

Throughout the text, we use atomic units: Planck's constant $\hbar = 1$, electron mass $m = 1$, and electron charge $e = -1$.

II. SETUP

First, we consider a focused Gaussian laser pulse propagating along the z direction. The finite duration of the pulse is taken into account by introducing an envelope function. In the paraxial approximation the explicit form of the external field reads (see, e.g., Ref. [8])

$$H_x(t,\boldsymbol{r}) = 0, \tag{1}$$

$$H_y(t,\boldsymbol{r}) = \frac{E_0\rho_0}{\rho(z)}\, f(\omega t - k_0 z)\exp\left[-\frac{x^2+y^2}{2\rho^2(z)}\right]\sin\phi, \tag{2}$$

$$H_z(t,\boldsymbol{r}) = \frac{E_0\rho_0 y}{k_0\rho_{\rm F}\rho^2(z)}\, f(\omega t - k_0 z)\exp\left[-\frac{x^2+y^2}{2\rho^2(z)}\right]\cos\tilde{\phi}, \tag{3}$$

$$E_x(t,\boldsymbol{r}) = H_y(t,\boldsymbol{r}), \tag{4}$$

$$E_y(t,\boldsymbol{r}) = 0, \tag{5}$$

$$E_z(t,\boldsymbol{r}) = \frac{E_0\rho_0 x}{k_0\rho_{\rm F}\rho^2(z)}\, f(\omega t - k_0 z)\exp\left[-\frac{x^2+y^2}{2\rho^2(z)}\right]\cos\tilde{\phi}, \tag{6}$$

where $k_0 \equiv 2\pi/\lambda$, $\rho(z) = \rho_0\sqrt{(1-z/\mathfrak{F})^2 + (z/z_*)^2}$,

$$\phi(t,\boldsymbol{r}) = \omega t - k_0 z + \arctan\frac{z\mathfrak{F}}{z_*(\mathfrak{F}-z)} + \pi\theta(z-\mathfrak{F}) - \frac{(x^2+y^2)[z+(z_*/\mathfrak{F})^2(z-\mathfrak{F})]}{2z_*\rho^2(z)} - \varphi, \tag{7}$$

$$\tilde{\phi}(t,\boldsymbol{r}) = \phi(t,\boldsymbol{r}) + \arctan\frac{z\mathfrak{F}}{z_*(\mathfrak{F}-z)} + \pi\theta(z-\mathfrak{F}) - \arctan\frac{z_*}{\mathfrak{F}}, \tag{8}$$

and $f(\xi)$ is a smooth envelope function containing $N_{\rm c}$ carrier cycles, $f(\xi) = \sin^2[\xi/(2N_{\rm c})]\theta(\pi N_{\rm c} - |\xi - \pi N_{\rm c}|)$. To specify the external field configuration, one has to define two more parameters in addition to the field amplitude E_0, wavelength λ, number of the carrier cycles $N_{\rm c}$, and the carrier-envelope phase (CEP) parameter φ. They can be, for example, the lens radius ρ_0 and focal length $\mathfrak{F}$. Using these quantities, one derives the remaining parameters:

$$z_* = k_0\rho_0^2, \tag{9}$$

$$z_{\rm F} = \frac{\mathfrak{F}}{1+\left[\mathfrak{F}/\left(k_0\rho_0^2\right)\right]^2}, \tag{10}$$

$$\rho_{\rm F} = \frac{\rho_0}{\sqrt{1+\left(k_0\rho_0^2/\mathfrak{F}\right)^2}}. \tag{11}$$

The field parameters are chosen as in Ref. [24]. In what follows, we assume $\lambda = 1.0\,\mu$m, $\varphi = 0$, $\rho_0 = 2.57\,\mu$m, and $\mathfrak{F} = 51.4\,\mu$m, which leads to $z_* = 41.5\,\mu$m, $z_{\rm F} = 20.3\,\mu$m, $\rho_{\rm F} = 2.0\,\mu$m, and $f_\# \equiv \mathfrak{F}/(2\rho_0) = 10.0$. The beam divergence reads

$$\Delta_0 = \sqrt{2}\lim_{z\to\infty}\frac{\rho(z)}{z} = \frac{\sqrt{2}}{k_0\rho_{\rm F}} \approx 0.11. \tag{12}$$

The number of carrier cycles is $N_{\rm c} = 10$, so the pulse duration is $\tau = \lambda N_{\rm c}/c = 33.3$ fs.

In what follows, we will examine a single laser pulse of the form defined above and a combination of two identical counterpropagating laser pulses. As will be demonstrated below, these two particular configurations already allow one to determine the laser intensity, covering a wide range of its possible values. We also underline that we are not primarily interested in maximizing the positron yield. For instance, while a single laser pulse produces a relatively small number of particles, it represents a more favorable setup for measuring very high intensities. We assume that one can initially guess the value of the laser intensity either from some rough estimates or from preliminary measurements according to our scheme. Then the field configuration should be adjusted in order to reduce the relative uncertainty.

For the seed particles, we will have two choices: either Xe atoms or free electrons distributed within the whole space with constant densities. The corresponding number densities amount to $n_{\rm Xe} = 10^{14}\,{\rm cm}^{-3}$ and $n_{\rm el} = 52 n_{\rm Xe}$, respectively. The factor of 52 takes into account that each Xe atom basically yields 52 electrons due to the ionization process. This choice of $n_{\rm Xe}$ and $n_{\rm el}$ allows one to judge whether the use of Xe atoms as the seed particles enhances the positron number.

III. THEORETICAL APPROACH

A common approach to a quantitative description of the pair-production process seeded by electrons is based on the particle-in-cell (PIC) method, where the particles are treated within the framework of classical relativistic mechanics. Photon emission and pair production can be incorporated by using closed-form local QED expressions. Basically, these QED rates are employed within Monte Carlo (MC) techniques. By performing a sufficient number of simulations, one can estimate, e.g., the total number of positrons created in the presence of strong laser pulses.

One of the major difficulties is properly describing the avalanchelike reaction which occurs when the particles produced again emit high-energy photons, initiating production

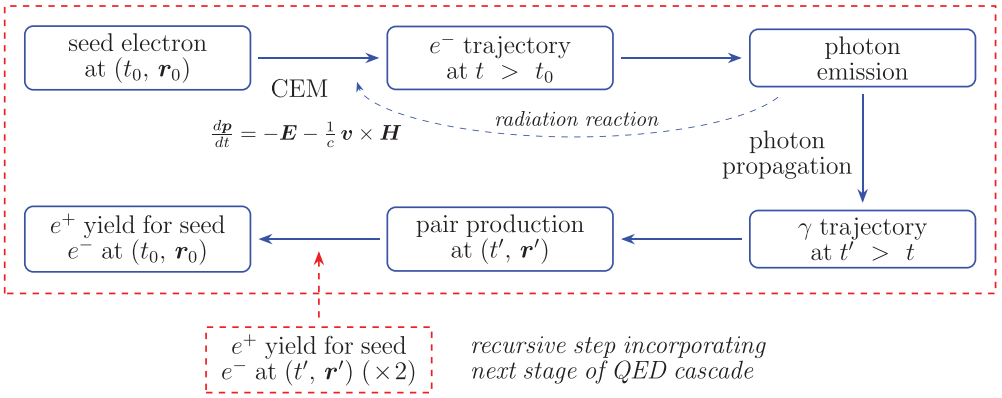

FIG. 1. Scheme of our numerical procedure taking into account pair production by the primary particles and QED cascade via a recursive approach. Here CEM stands for classical equations of motion.

of new pairs [26–31]. However, within the MC approach, the secondary particles can be treated quite straightforwardly.

On the other hand, at least the first stages of the cascade can be treated in a deterministic way, i.e., without MC calculations. This approach was used in Ref. [24], where we incorporated photon emission only by the primary particles. The computational algorithm is briefly outlined in Fig. 1 (see dashed box). In the case of Xe atoms, we first consider the ionization process in the presence of the external laser field and then evolve the corresponding "electrons" (macroparticles) obtained at each time step as seed particles, taking into account their probability weight (the ionization model is described in Appendix A). Unlike the weakly bound electrons, the inner-shell electrons do not get ionized immediately, so the external Lorentz force starts to accelerate them at later times, when the field strength gets closer to its maximal value [32]. Therefore, such seed particles basically achieve larger values of energy and generate more pairs [24]. In Ref. [24], we argued that the cascade mechanism can be neglected in the vicinity of the threshold, where the diagnostics is particularly efficient. However, it was not that clear to what extent one can widen this vicinity before the cascade mechanism comes into play. Here we will estimate the contribution of the later stages.

We assume that the momenta of the electron and positron created in multiphoton Breit-Wheeler pair production are parallel to that of the photon and the electron has energy $\varepsilon_{\rm el}$. The function controlling the distribution of the photon energy ε_γ between the electron and positron in the pair reads [33] $(0 < f_{\rm el} \equiv \varepsilon_{\rm el}/\varepsilon_\gamma < 1)$

$$p_f(f_{\rm el}, \chi) = \frac{2 + f_{\rm el}(1 - f_{\rm el})}{f_{\rm el}(1 - f_{\rm el})} K_{2/3}\left[\frac{1}{3\chi f_{\rm el}(1 - f_{\rm el})}\right] \frac{1}{k(\chi)}, \tag{13}$$

where $\chi \equiv |F_{\mu\nu}k^\nu|/(2c^4)$, k^ν is the photon four-momentum, and $k(\chi)$ is a normalization constant. This distribution function is symmetric about $f = 1/2$. To obtain order-of-magnitude estimates, we first assume that $f = 1/2$ and evolve only the electron trajectory, multiplying the results by a factor of 2. The electron travels in the external field and emits photons. We do not take into account small probabilities and low-energy photons in order to save computational time. This also allows us to efficiently incorporate the second stage of the cascade in the regime where it does not contribute much. Nevertheless, while we do not follow the dynamics of the low-energy photons, we take into account the corresponding radiation reaction, i.e., momentum transfer from the electron to the photons regardless of whatever energy the latter have.

In our simulations, the electron trajectories are obtained in the presence of the electromagnetic field given by Eqs. (1)–(6) and the radiation-reaction effects. However, we disregard the fact that the external background is modified because the seed particles and pairs produced also generate electromagnetic fields. Since we propagate the seed macroparticles one by one, it is difficult to incorporate the interparticle interaction, although within modern PIC simulations it is done quite straightforwardly. This issue represents an evident shortcoming of our approach, so the corresponding uncertainties have to be estimated. To this end, we performed a direct benchmarking of our technique against PIC simulations (see Appendix B). According to our results, the effects of the field modification for our setup do not affect the positron yield below the cascade threshold much. Note that in Ref. [34] this issue was discussed in detail, and it was demonstrated that the laser energy is efficiently absorbed only for larger durations of the external field and higher intensities compared to the field parameters used in our study (see also Ref. [35]).

To incorporate the QED cascade, we carry out the following recursive procedure. First, we calculate the contributions to the positron yield from each space-time point $(t_0, \boldsymbol{r}_0)$ according to the scheme displayed in the upper dashed box in Fig. 1. Here we also vary the energy and direction of the seed electrons to use this information in the subsequent recursive steps. Second, we recursively update the data by adding the second-stage contributions at the time-space position $(t', \boldsymbol{r}')$ using the results tabulated within the first step of our technique. These additional terms are multiplied by 2 since both the electron and positron represent secondary particles. Updating the data according to this recursive procedure, we take into account the later cascade stages one by one. These additional steps consume an almost negligible amount of computational time.

Finally, let us briefly discuss the validity of the locally constant field approximation (LCFA), which is employed throughout our simulations in order to compute the QED rates of the photon emission and pair-production processes.

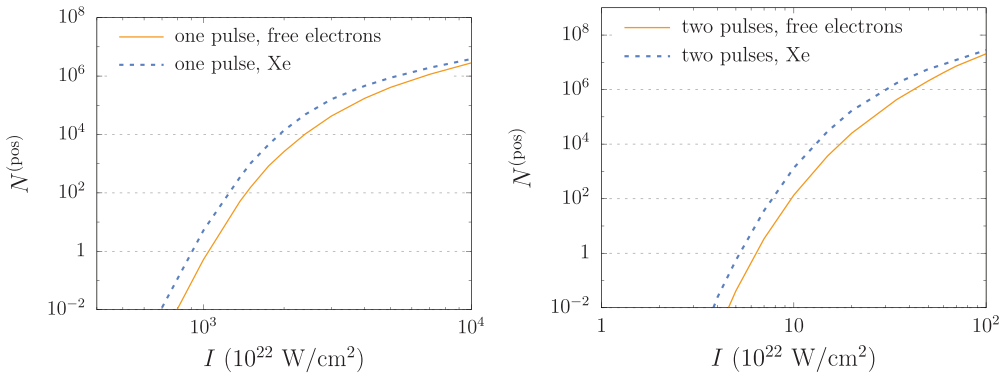

FIG. 2. Total number of positrons produced in an individual laser pulse (left) and the combination of two counterpropagating laser pulses (right) as a function of the laser intensity I. The seed particles are either free electrons (solid lines) or neutral Xe atoms (dashed lines). The numerical simulations incorporate pair production by primary particles and the subsequent QED cascade process.

The general idea of the LCFA is that the QED rates do not depend on the specific structure of the external field, provided that the field strength is smaller than the Schwinger critical value, the photon parameter $\chi = |F_{\mu\nu}k^\nu|/(2c^4)$ and the electron parameter $\eta = |F_{\mu\nu}p^\nu|/c^4$ are sufficiently large, and the dimensionless parameter $a_0 = E_0/(c\omega)$ obeys $a_0 \gg 1$ [36]. This means that one can describe the necessary QED processes and choose the most convenient scenario. Basically, one considers either a constant crossed field [36,37] or a static magnetic field [38]. In the present study, we choose the latter configuration, following the emission and pair-production model employed in, e.g., Refs. [24,29,39–41]. For the laser intensities considered in our study, the field amplitude E_0 is always much smaller than the Schwinger limit, $E_0 \ll E_c$, and the condition $a_0 \gg 1$ is also satisfied in the spatiotemporal regions where the QED rates are not negligible. To provide a noticeable number of particles, the seed electrons and the photons emitted should have sufficiently large values of the η and χ parameters. Accordingly, to compute the corresponding rates of photon emission and pair production, one can utilize the LCFA. We also note that in the case of nonlinear Compton scattering, the LCFA is very accurate in the domain of relatively high photon energies [42,43]. Although the LCFA may overestimate the photon yield in the low-energy region, these soft photons can be disregarded since the subsequent Breit-Wheeler process is likely to occur only when the photon energy is high. A detailed analysis of the validity of the LCFA in the context of various QED processes can be found in recent papers [42–51] and the references therein.

IV. RESULTS

A. Cascade threshold: Estimates

First, let us provide simple estimates of the cascade threshold. Although general expressions were already derived in Ref. [27], we will employ the criteria from Ref. [31], where the case of a single focused laser pulse was examined explicitly. According to Ref. [31], the avalanchelike cascade process can occur if the following two conditions are satisfied:

$$\mu \gtrsim \frac{1}{2\sqrt{2}\Delta_0}, \tag{14}$$

$$\mu \gtrsim \frac{1}{2\sqrt{2}\pi^4 \varkappa^4 \Delta_0^7}, \tag{15}$$

where $\varkappa \equiv (17\sqrt{2}\alpha^2 c^2/\omega)^{1/2}$. For the field parameters we have chosen, we obtain

$$E_0 \gtrsim 0.043 E_c, \tag{16}$$

$$E_0 \gtrsim 0.034 E_c. \tag{17}$$

It turns out that the first condition is more restrictive. It yields the following threshold value of the laser intensity: $I_{\mathrm{thr}} \approx 4 \times 10^{26}\,\mathrm{W/cm^2}$. The crucial point is that notable positron generation appears for sufficiently lower laser intensity on the level of $10^{25}\,\mathrm{W/cm^2}$ [24]. Since our diagnostic scheme is most accurate in the vicinity of this threshold, it suggests that one does not need to incorporate the cascade effects while predicting the positron yield. Nevertheless, this should be directly confirmed by numerical calculations, so that one clearly demonstrates to what extent one can rely on the results while taking into account pair production by only the primary particles.

In the case of two counterpropagating laser pulses, the threshold values of the laser intensity for both positron production and the avalanchelike reaction are substantially lower because the external field configuration is more inhomogeneous. However, one may expect that the two corresponding threshold values of the laser intensity still differ by an order of magnitude. A quantitative analysis of both external field configurations (single pulse and two pulses) will be performed next.

B. Numerical analysis

In Fig. 2 we present the results for the total positron yield as a function of the laser intensity, taking into account the QED cascade contribution. In the case of two pulses, the intensity I is that of an individual pulse. These data allow one to localize the intensity domain where a notable number of positrons are produced. Note that the function $N^{(\mathrm{pos})}(I)$ exhibits a threshold behavior, so that one can accurately recover the laser intensity even if the positron yield is known only on the order-of-magnitude level [24]. As was demonstrated in Ref. [24], the relative uncertainty is on the level of 10% in the vicinity of the pair-production threshold.

The curves in Fig. 2 displayed on a logarithmic scale are almost indistinguishable from those presented in Ref. [24],

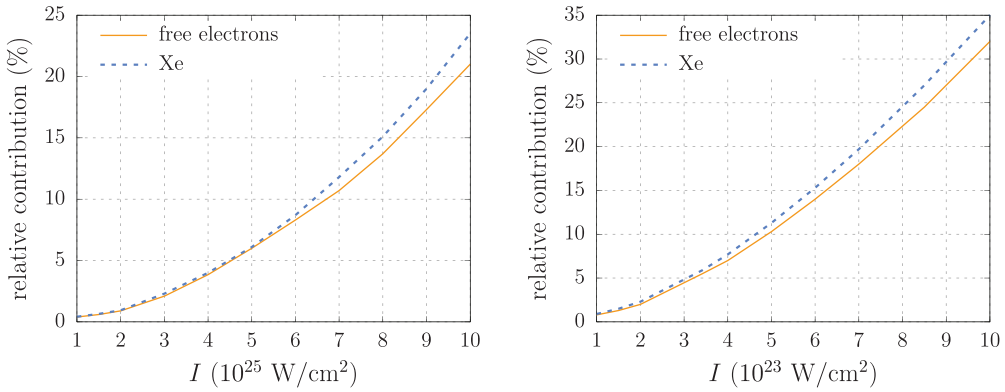

FIG. 3. Relative contribution of the cascade process as a function of the laser intensity in the case of a single laser pulse (left) and two counterpropagating laser pulses (right).

where the QED cascade was completely disregarded. To quantitatively analyze the role of the later stages, in Fig. 3 we display the relative contribution of the QED cascade to the total number of positrons. We observe that in the vicinity of the threshold of positron generation, the cascade process yields a negligible contribution. The later stages become important only when the intensity is sufficiently high. On the other hand, this corresponds to the intensity domain where the number of positrons is already very large and the function $N^{(\mathrm{pos})}(I)$ no longer has a large slope (see Fig. 2). These results confirm that there is, indeed, an extended intensity domain where one can effectively generate positrons and measure the laser intensity without taking into account the cascade effects. This is the main finding of the present paper.

We note that although for sufficiently high laser intensities the total number of particles can be very large, this does not necessarily mean that the QED cascade is also important. Here we should clarify the concept of a cascade. In Ref. [31] the authors defined the cascade threshold by requiring that a single electron produce one pair (via the two-stage process) per laser half-period. Although the particle yield can be easily enhanced by increasing the density n of the seed electrons, the cascade contribution will be enhanced by the same numerical factor, so the *absolute* value $N^{(\mathrm{pos})}$ does not contain any information on the *relative* contribution of the later cascade stages. To better understand whether the particle number $N^{(\mathrm{pos})}$ is large, one can also compare it with the number of initial seed electrons within the interaction region, which can be roughly estimated via

$$N_0 \sim \pi \rho_{\mathrm{F}}^2 |z_* - z_{\mathrm{F}}| n_{\mathrm{el}} \sim 10^6. \tag{18}$$

Let us compare our results with those presented in Ref. [52]. According to three-dimensional PIC simulations carried out in Ref. [52], 100 electrons initially placed in the focal plane in the case of two counterpropagating laser pulses with $I = 3.5 \times 10^{23}\,\mathrm{W/cm^2}$ produce about 0.03 pair per electron. Our numerical approach yields 7×10^3 pairs for this laser intensity, so the ratio $N^{(\mathrm{pos})}/N_0$ amounts approximately to 0.01, which is several times smaller. First, we note that while the pulse duration in our study is almost the same as in Ref. [52], the beam geometry is a bit different. Namely, the beam waist is 1.6 times larger than in our simulations, and the pulse envelope and the way of focusing are also different. Second, the seed particles considered in Ref. [52] are located in the central region where the laser-field amplitude is maximal. On the other hand, in our setup only a certain fraction of the seed electrons distributed uniformly can efficiently interact with the laser field. It is evident that by placing 100 electrons far from the focal plane, one will obtain a considerably smaller number of pairs. This also suggests that the cascade threshold depends not only on the field configuration but also on the spatial distribution of the seed particles. Moreover, Ref. [52] also found that for $I = 6.8 \times 10^{23}\,\mathrm{W/cm^2}$ the particle yield is 30 pairs per electron (the only seed electron was located at the center of the focal plane). Our simulations yield $N^{(\mathrm{pos})}/N_0$ of the order of 0.1, which is already 2 orders of magnitude smaller. Within this comparison, we can also say that the value N_0 in Eq. (18) represents only an extremely rough estimate given the different setups in Ref. [52] and in our study. On the one hand, replacing the value (18) with the "effective" number of seed electrons $N_0 = 2.3 \times 10^4$ makes our predictions coincide. However, in order to *directly* benchmark our technique against PIC simulations, we performed additional computations by employing the field configuration from Ref. [52] (see Appendix B).

Finally, we note that using neutral Xe atoms as seed particles with density $n_{\mathrm{Xe}} = 10^{14}\,\mathrm{cm^{-3}}$, we can enhance the particle yield. Nevertheless, the relative contribution of the QED cascade remains at the same level.

C. Laser-beam divergence

Here we will vary the beam divergence Δ_0 by changing ρ_0 while keeping the other parameters (E_0, λ, $\mathfrak{F}$) the same. We are mainly interested in the Δ_0 dependence of the pair-production threshold. We find the laser intensity I_{thr} which ensures production of 100 positrons as a function of Δ_0. The results are presented in Fig. 4 for both a single laser pulse (left) and two pulses (right). We observe that by increasing the laser-beam divergence, we can further lower the particle-production threshold. Not only does this make the setup more efficient in terms of positron generation, but the diagnostic scheme also becomes more flexible. The laser-beam parameters, i.e., the lens radius or its optical power, allow one to shift the pair-production threshold to lower or higher intensities in order to

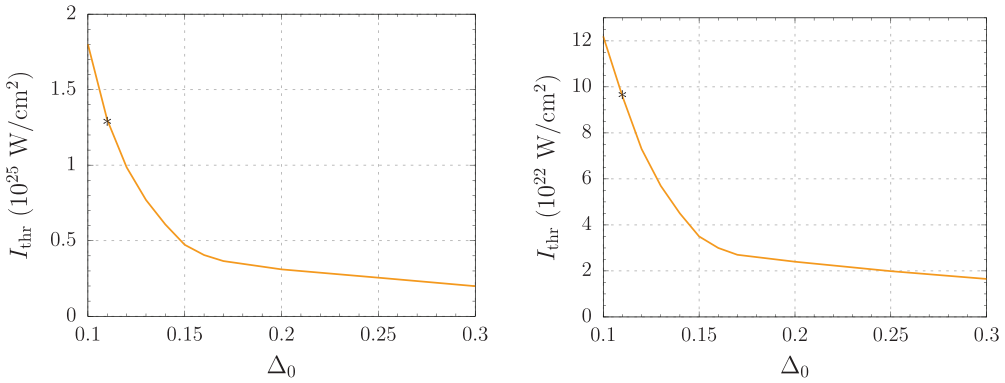

FIG. 4. Threshold values of the laser intensity for generating 100 positrons in the case of a single laser pulse (left) and two counterpropagating laser pulses (right) as a function of Δ_0 for $\lambda = 1.0\,\mu$m and $\mathfrak{F} = 51.4\,\mu$m. The seed particles are free electrons with number density $n_{\rm el} = 52 \times 10^{14}\,{\rm cm}^{-3}$. The stars correspond to the value $\Delta_0 = 0.11$ ($\rho_0 = 2.57\,\mu$m) used in the previous simulations.

adjust the setup for measuring a given laser intensity with a minimal uncertainty.

In the case of two counterpropagating laser pulses, the relative angle between the laser beams is $\theta = \pi$. The scenario involving a single laser pulse can be viewed as a combination of two coherent pulses with $\theta = 0$ (note that each of the pulses then has intensity $I/4$, so the threshold values of the laser intensity in the two setups should be compared while accounting for a factor of 4). The essential point here is that when varying the angle θ, one should expect that the particle yield (and, accordingly, the intensity threshold) will cover the whole intermediate interval between the two limiting cases examined in our study. This allows one to make the diagnostics even more adjustable and better control the position of the threshold with respect to the laser-field amplitude. Performing computations for intermediate values of θ is an important prospect for our future studies.

V. CONCLUSION

In this study we performed a numerical analysis of the process of positron generation in strong laser fields. It turned out that one can determine the laser intensity by measuring the positron yield with a relative uncertainty on the level of 10% in a wide range of intensities from 10^{23} to $10^{26}\,{\rm W/cm}^2$ depending on the laser-field configuration. By modifying our previously developed technique, we took into account the QED cascade processes, improving the accuracy of our diagnostic scheme. It was demonstrated that there is an extended domain of the laser intensity where the cascade contribution is insignificant while the number of positrons produced is already sufficiently large to be measured. Adjusting the laser-field configuration so that the preliminary guess of the (as yet unknown) intensity is close to the pair-production threshold, one can accurately extract the intensity. One of the key degrees of freedom here is the geometry of the laser beams. In the present study, we obtained theoretical predictions for the positron yield depending on the divergence parameter, which is also expected to be helpful within experimental investigations. Varying the laser-field polarization is then an important task for our future studies (see, e.g., Ref. [53]). Another interesting feature which can also be computed by means of our numerical technique is the angular distribution of positrons (see, e.g., Refs. [53,54]).

ACKNOWLEDGMENT

This study was funded by the Russian Science Foundation (Grant No. 23-12-00012).

APPENDIX A: IONIZATION MODEL

Here we will briefly describe how we compute the necessary ionization rates at the stage when atoms interacting with a strong laser background produce seed electrons. For a given atom having position $\boldsymbol{r}_0$, we assume that after ionization the free electrons appear at rest at the same point $\boldsymbol{r}_0$ and start to accelerate in the external laser field. First, we evolve in time the ionization probabilities P_j for each electron level j via

$$dP_j(t) = [1 - P_j(t)]W_j(t)dt, \quad j = 1, 2, \ldots, N_{\rm lev}, \tag{A1}$$

where $W_j(t)$ is the ionization rate depending on j, the effective charge $Z_j(t)$, and the local electric field strength $E(t) \equiv E(\boldsymbol{r}_0, t)$. At each time instant t, we recalculate the charge according to

$$Z_j(t) = j + \sum_{k=j+1}^{N_{\rm lev}} P_k(t); \tag{A2}$$

i.e., we take into account the reduction of the screening effects. Our goal here is to properly estimate the ionization rate $W(t)$. Let us omit j considering a given energy level. We use the NIST database [55] to obtain the corresponding ionization potential I_p. We also introduce the following quantities:

$$\kappa = \sqrt{2I_p}, \tag{A3}$$

$$\nu = Z/\kappa, \tag{A4}$$

$$\mathcal{F}(t) = |E(t)|/\kappa^3. \tag{A5}$$

As the Keldysh parameter $\gamma_{\rm K} = \sqrt{2I_p}\omega/|E|$ is very small, $\gamma_{\rm K} \lesssim 10^{-3}$, we utilize the ionization model describing tunnel ionization in the form of the Ammosov-Delone-Krainov

(ADK) approach [56]:

$$W_{\mathrm{ADK}}(t) = \frac{|E(t)|}{8\pi Z}\sqrt{\frac{3\mathcal{F}(t)}{\pi}}\left(\frac{4\mathrm{e}}{\nu\mathcal{F}(t)}\right)^{2\nu}\exp\left(-\frac{2}{3\mathcal{F}(t)}\right). \tag{A6}$$

It is well known that this technique requires corrections in the regime of low ionization potential. The corresponding barrier-suppression (BS) effects should be taken into account (see, e.g., Refs. [5,57–60]). The characteristic BS field is $\mathcal{F}_{\mathrm{BS}} = 1/(16\nu)$ [59]. As in our previous study [24], we opt to use the method proposed in Ref. [58]. Using the ADK model, we compute the ionization rates according to

$$W(t) = \begin{cases} W_{\mathrm{ADK}}(t) & \text{if } \mathcal{F} < \mathcal{F}_{\mathrm{BS}}, \\ W_{\mathrm{ADK}}(t)\exp[-2\overline{\alpha}\nu^2\mathcal{F}(t)] & \text{if } \mathcal{F}_{\mathrm{BS}} \leqslant \mathcal{F}(t) \leqslant \mathcal{F}_{\mathrm{L}}, \\ W_{\mathrm{L}}(t) & \text{if } \mathcal{F} > \mathcal{F}_{\mathrm{L}}, \end{cases} \tag{A7}$$

where $W_{\mathrm{L}}(t) = 2I_p\mathcal{F}(t)$ and $\mathcal{F}_{\mathrm{L}}$ is chosen so that the function (A7) is continuous. The crucial point here for preserving the high accuracy of our computations is the fact that the barrier-suppression regime corresponds to ionization of the outer-shell electrons, which get ionized immediately due to the very high field amplitudes considered in the present study.

APPENDIX B: BENCHMARKING AGAINST PIC CODES: GROWTH RATE

Here we will employ our technique based on a deterministic approach rather than Monte Carlo method in order to compare our predictions with those presented in Ref. [52]. In particular, we will assess the effect of the external field modification due to the presence of the charge and current densities, which is neglected in our simulations. We expect that these effects are insignificant below the cascade threshold, where we propose to use our diagnostic scheme.

In Ref. [52] the (possible) cascade process was quantitatively described in terms of the so-called growth rate (GR) Γ, allowing one to approximate the temporal evolution of the positron number via $N^{(\mathrm{pos})}(t) \sim \exp(\Gamma t)$ (see also Refs. [26,28,34,61]). Since within our numerical approach, we separately evolve electron trajectories, it is difficult to construct the function $N^{(\mathrm{pos})}(t)$, and we always compute only the final number of positrons $N^{(\mathrm{pos})}$. Nevertheless, we can use the final values of $N^{(\mathrm{pos})}$ to identify the GR via

$$N^{(\mathrm{pos})} = N_0\mathrm{e}^{\Gamma\tau} - N_0 \tag{B1}$$

and directly compare it with the results of Ref. [52]. Here we point out that the process duration τ in Eq. (B1) may differ from the pulse duration or, equivalently, the preexponential factor N_0 may differ from the real number of seed particles since the function $N^{(\mathrm{pos})}(t)$ starts to grow exponentially for sufficiently large t (see, e.g., Fig. 3(b) in Ref. [52]). To take this into account and confirm that our simulations yield correct predictions within a window of 1 order of magnitude, we will assume that τ in Eq. (B1) exactly corresponds to the laser pulse duration, while N_0 will be varied from $100/\sqrt{10}$ to $100\sqrt{10}$, where 100 is the real number of the seed electrons according to the initial distribution used in Ref. [52]. In what follows, we will determine whether the GRs from Ref. [52] lie in the corresponding region.

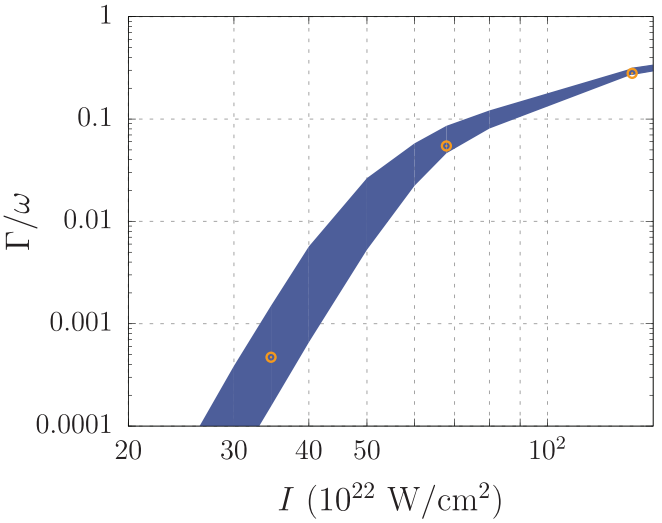

FIG. 5. Ratio Γ/ω ($\omega = 2\pi c/\lambda$, $\lambda = 1\,\mu$m) computed using our approach (blue region) and the values extracted from the PIC simulations performed in Ref. [52] (orange points).

In Fig. 5 we display estimates of the GR as a function of the laser intensity for the setup from Ref. [52]. The seed particles are 100 electrons located within the focal plane. We observe that our predictions are in agreement with the results of PIC simulations. The intensity region in Fig. 5 also includes the onset of the QED cascade corresponding to $I \gtrsim 7 \times 10^{23}\,\mathrm{W/cm^2}$ [52]. For such high intensities, one has to take into account the external field modification and the transfer of its energy to the particles produced (see, e.g., Refs. [34,35]). Moreover, to describe prolific pair production by means of our approach, we have to perform a considerably larger number of computations, so that the results are converged with respect to the spatiotemporal resolution of the numerical grids, where we discretize the electron trajectories. Accordingly, we refrain from calculating the positron yield in the regime of a fully developed QED cascade. Here we underline that this is unnecessary for our diagnostic method as a quite large number of positrons can already be generated in the domain of lower laser intensities.

We also note that in the setup considered in Figs. 2 and 3, we did not identify the cascade threshold, which suggests that the corresponding field configuration is less effective than that considered in this Appendix. Reference [52] argued that the cascade threshold can be identified by means of the relation $\Gamma\rho_{\mathrm{F}}/c = 1$, so for a given field amplitude E_0, smaller values of the beam waist require larger GRs and thus higher intensity. Since here $\rho_{\mathrm{F}} = 3.2\,\mu$m as in Ref. [52], which is 1.6 times larger than the beam waist of the laser beam in Figs. 2 and 3, the cascade threshold in the latter case is shifted to the region of higher intensities, $I > 10^{24}\,\mathrm{W/cm^2}$.

[1] J. W. Yoon *et al.*, Optica **8**, 630 (2021).
[2] A. Fedotov, A. Ilderton, F. Karbstein, B. King, D. Seipt, H. Taya, and G. Torgrimsson, Phys. Rep. **1010**, 1 (2023).
[3] A. Gonoskov, T. G. Blackburn, M. Marklund, and S. S. Bulanov, Rev. Mod. Phys. **94**, 045001 (2022).
[4] M. F. Ciappina, S. V. Popruzhenko, S. V. Bulanov, T. Ditmire, G. Korn, and S. Weber, Phys. Rev. A **99**, 043405 (2019).
[5] M. F. Ciappina and S. V. Popruzhenko, Laser Phys. Lett. **17**, 025301 (2020).
[6] M. F. Ciappina, E. E. Peganov, and S. V. Popruzhenko, Matter Radiat. Extremes **5**, 044401 (2020).
[7] O. Har-Shemesh and A. Di Piazza, Opt. Lett. **37**, 1352 (2012).
[8] O. E. Vais, S. G. Bochkarev, and V. Yu. Bychenkov, Plasma Phys. Rep. **42**, 818 (2016).
[9] W. Yan, C. Fruhling, G. Golovin, D. Haden, J. Luo, P. Zhang, B. Zhao, J. Zhang, C. Liu, M. Chen, S. Chen, S. Banerjee, and D. Umstadter, Nat. Photon. **11**, 514 (2017).
[10] C. N. Harvey, Phys. Rev. Accel. Beams **21**, 114001 (2018).
[11] C. Z. He, A. Longman, J. A. Pérez-Hernández, M. de Marco, C. Salgado, G. Zeraouli, G. Gatti, L. Roso, R. Fedosejevs, and W. T. Hill, Opt. Express **27**, 30020 (2019).
[12] T. G. Blackburn, E. Gerstmayr, S. P. D. Mangles, and M. Marklund, Phys. Rev. Accel. Beams **23**, 064001 (2020).
[13] Z. W. Lu, X. D. Hou, F. Wan, Y. I. Salamin, C. Lv, B. Zhang, F. Wang, Z. F. Xu, and J. X. Li, Matter Radiat. Extremes **8**, 034401 (2023).
[14] M. Kalashnikov, A. Andreev, K. Ivanov, A. Galkin, V. Korobkin, M. Romanovsky, O. Shiryaev, M. Schnuerer, J. Braenzel, and V. Trofimov, Laser Part. Beams **33**, 361 (2015).
[15] O. E. Vais, S. G. Bochkarev, S. Ter-Avetisyan, and V. Yu. Bychenkov, Quantum Electron. **47**, 38 (2017).
[16] O. E. Vais and V. Yu. Bychenkov, Appl. Phys. B **124**, 211 (2018).
[17] K. A. Ivanov, I. N. Tsymbalov, O. E. Vais, S. G. Bochkarev, R. V. Volkov, V. Yu. Bychenkov, and A. B. Savel'ev, Plasma Phys. Controlled Fusion **60**, 105011 (2018).
[18] K. Krajewska, F. Cajiao Vélez, and J. Z. Kamiński, Plasma Phys. Controlled Fusion **61**, 074004 (2019).
[19] F. Mackenroth, A. R. Holkundkar, and H.-P. Schlenvoigt, New J. Phys. **21**, 123028 (2019).
[20] O. E. Vais, A. G. R. Thomas, A. M. Maksimchuk, K. Krushelnick, and V. Yu. Bychenkov, New J. Phys. **22**, 023003 (2020).
[21] O. E. Vais and V. Yu. Bychenkov, Plasma Phys. Controlled Fusion **63**, 014002 (2021).
[22] A. Longman, S. Ravichandran, L. Manzo, C. Z. He, R. Lera, N. McLane, M. Huault, G. Tiscareno, D. Hanggi, P. Spingola, N. Czapla, R. L. Daskalova, L. Roso, R. Fedosejevs, and W. T. Hill, Phys. Plasmas **30**, 082110 (2023).
[23] N. D. Bukharskii, O. E. Vais, Ph. A. Korneev, and V. Yu. Bychenkov, Matter Radiat. Extremes **8**, 014404 (2023).
[24] I. A. Aleksandrov and A. A. Andreev, Phys. Rev. A **104**, 052801 (2021).
[25] A. Di Piazza, C. Müller, K. Z. Hatsagortsyan, and C. H. Keitel, Rev. Mod. Phys. **84**, 1177 (2012).
[26] A. M. Fedotov, N. B. Narozhny, G. Mourou, and G. Korn, Phys. Rev. Lett. **105**, 080402 (2010).
[27] N. B. Narozhny and A. M. Fedotov, Phys.-Usp. **58**, 95 (2015).
[28] A. R. Bell and J. G. Kirk, Phys. Rev. Lett. **101**, 200403 (2008).
[29] J. G. Kirk, A. R. Bell, and I. Arka, Plasma Phys. Controlled Fusion **51**, 085008 (2009).
[30] N. V. Elkina, A. M. Fedotov, I. Yu. Kostyukov, M. V. Legkov, N. B. Narozhny, E. N. Nerush, and H. Ruhl, Phys. Rev. Spec. Top. Accel. Beams **14**, 054401 (2011).
[31] A. A. Mironov, E. G. Gelfer, and A. M. Fedotov, Phys. Rev. A **104**, 012221 (2021).
[32] S. X. Hu and A. F. Starace, Phys. Rev. E **73**, 066502 (2006).
[33] J. K. Daugherty and A. K. Harding, Astrophys. J. **273**, 761 (1983).
[34] T. Grismayer, M. Vranic, J. L. Martins, R. A. Fonseca, and L. O. Silva, Phys. Plasmas **23**, 056706 (2016).
[35] E. N. Nerush, I. Yu. Kostyukov, A. M. Fedotov, N. B. Narozhny, N. V. Elkina, and H. Ruhl, Phys. Rev. Lett. **106**, 035001 (2011).
[36] A. I. Nikishov and V. I. Ritus, Sov. Phys. JETP **19**, 529 (1964).
[37] V. I. Ritus, J. Russ. Laser Res. **6**, 497 (1985).
[38] T. Erber, Rev. Mod. Phys. **38**, 626 (1966).
[39] R. Duclous, J. G. Kirk, and A. R. Bell, Plasma Phys. Controlled Fusion **53**, 015009 (2011).
[40] C. P. Ridgers, J. G. Kirk, R. Duclous, T. Blackburn, C. S. Brady, K. Bennett, T. D. Arber, and A. R. Bell, J. Comput. Phys. **260**, 273 (2014).
[41] T. D. Arber, K. Bennett, C. S. Brady, A. Lawrence-Douglas, M. G. Ramsay, N. J. Sircombe, P. Gillies, R. G. Evans, H. Schmitz, A. R. Bell, and C. P. Ridgers, Plasma Phys. Controlled Fusion **57**, 113001 (2015).
[42] A. Di Piazza, M. Tamburini, S. Meuren, and C. H. Keitel, Phys. Rev. A **99**, 022125 (2019).
[43] A. Ilderton, B. King, and D. Seipt, Phys. Rev. A **99**, 042121 (2019).
[44] S. Meuren, C. H. Keitel, and A. Di Piazza, Phys. Rev. D **93**, 085028 (2016).
[45] T. G. Blackburn, D. Seipt, S. S. Bulanov, and M. Marklund, Phys. Plasmas **25**, 083108 (2018).
[46] I. A. Aleksandrov, G. Plunien, and V. M. Shabaev, Phys. Rev. D **99**, 016020 (2019).
[47] D. G. Sevostyanov, I. A. Aleksandrov, G. Plunien, and V. M. Shabaev, Phys. Rev. D **104**, 076014 (2021).
[48] Q. Z. Lv, E. Raicher, C. H. Keitel, and K. Z. Hatsagortsyan, Phys. Rev. Res. **3**, 013214 (2021).
[49] E. G. Gelfer, A. M. Fedotov, A. A. Mironov, and S. Weber, Phys. Rev. D **106**, 056013 (2022).
[50] I. A. Aleksandrov, D. G. Sevostyanov, and V. M. Shabaev, Symmetry **14**, 2444 (2022).
[51] I. A. Aleksandrov and V. M. Shabaev, arXiv:2303.16273.
[52] T. Grismayer, M. Vranic, J. L. Martins, R. A. Fonseca, and L. O. Silva, Phys. Rev. E **95**, 023210 (2017).
[53] A. Mercuri-Baron, M. Grech, F. Niel, A. Grassi, M. Lobet, A. Di Piazza, and C. Riconda, New J. Phys. **23**, 085006 (2021).
[54] S. Tiwary and N. Kumar, Phys. Rev. Res. **3**, 043190 (2021).
[55] NIST, https://physics.nist.gov/PhysRefData/ASD/ionEnergy.html.

[56] M. V. Ammosov, N. B. Delone, and V. P. Krainov, Zh. Eksp. Teor. Fiz. **91**, 2008 (1986) [Sov. Phys. JETP **64**, 1191 (1986)].
[57] V. P. Krainov, J. Opt. Soc. Am. B **14**, 425 (1997).
[58] I. I. Artemenko and I. Yu. Kostyukov, Phys. Rev. A **96**, 032106 (2017).
[59] X. M. Tong and C. D. Lin, J. Phys. B **38**, 2593 (2005).
[60] Q. Zhang, P. Lan, and P. Lu, Phys. Rev. A **90**, 043410 (2014).
[61] V. F. Bashmakov, E. N. Nerush, I. Yu. Kostyukov, A. M. Fedotov, and N. B. Narozhny, Phys. Plasmas **21**, 013105 (2014).